Determination of nucleation and growth rates from observation of a SO_2 induced atmospheric nucleation event

Bart Verheggen and Michael Mozurkewich

Department of Chemistry and Centre for Atmospheric Chemistry, York University, Toronto, Ontario, Canada

Received 27 March 2001; revised 20 July 2001; accepted 20 August 2001; published 12 June 2002.

[1] A method to determine the particle nucleation rate directly from atmospheric measurements is presented. During the Southern Ontario Oxidant Study (SONTOS) field campaign in rural Ontario, Canada, particle size distributions and concentrations of a range of photochemical species were measured. On 25 August 1993, the size distribution showed a pronounced peak in the concentration of nucleation mode particles. This correlated with, but lagged behind, a peak in the SO_2 concentration. The data imply that nucleation occurred aloft as an SO_2 plume was entrained into the growing boundary layer. The particle growth rates were determined from the evolution of the measured particle size distributions, while accounting for coagulation and dilution. In principle, measurements of precursor species are not needed. However, in this case study, the ground-based measurements did not reflect the aerosol concentrations in the plume aloft; as a result, extrapolation of the growth rate was necessary. This was accomplished by using a one-dimensional model to calculate the gas phase sulfuric acid concentration. The particle growth rate due to condensation of H_2SO_4 was calculated and used to extrapolate the observed growth backward to obtain the time of formation. From the particle number in a certain size interval, suitably corrected for losses by coagulation and dilution, and the time interval in which they formed, the nucleation rate can be determined. We obtained nucleation rates of 5–40 cm^{-3} s^{-1} for sulfuric acid mixing ratios of 3–10 pptv. These nucleation rates are higher than predicted by classical binary nucleation theory for H_2SO_4 and H_2O. *INDEX TERMS:* 0305 Atmospheric Composition and Structure: Aerosols and particles (0345, 4801); 0365 Atmospheric Composition and Structure: Troposphere—composition and chemistry; 0345 Atmospheric Composition and Structure: Pollution—urban and regional (0305)

1. Introduction

[2] The radiative effects of the atmospheric aerosol are responsible for a large amount of uncertainty in assessing climate change [*Schwartz*, 1996; *Intergovernmental Panel on Climate Change (IPCC)*, 1995]. Both direct climate forcing (scattering and absorption of radiation by particles) and indirect forcing (modifying radiative properties of clouds) are influenced by particle size, composition and relative humidity [*Nemesure et al.*, 1995; *Pilinis et al.*, 1995; *Twomey*, 1991; *Leaitch et al.*, 1992, 1996]. Particle nucleation and growth influence both the size distribution and the composition of the aerosol. Homogeneous nucleation of sulfuric acid and water is thought to be a major source of new particles [*Andronache et al.*, 1997; *Weber et al.*, 1997] although recently biogenic emissions have also been proposed to play a role in particle formation [*Leaitch et al.*, 1999; *Weber et al.*, 1998].

[3] Particle nucleation is an extremely difficult process to quantify because of its nonlinear nature. This is clearly shown by the large discrepancies between measurements (both laboratory and atmospheric) and classical nucleation theory; these discrepancies often amount to several orders of magnitude [*Weber et al.*, 1995, 1997, 1998; *Wyslouzil et al.*, 1991; *Andronache et al.*, 1997]. Different parameterizations of nucleation rates give orders of magnitude different results [*Kulmala and Laaksonen*, 1990]. Good agreement of theoretical nucleation rates with laboratory experiments has been presented [*Viisanen et al.*, 1997], but the sulfuric acid concentrations used were much higher than is typical for the atmosphere. Since the nucleation rate is extremely sensitive to the sulfuric acid concentration, extrapolation to atmospheric values is highly uncertain.

[4] *Weber et al.* [1997, 1998] hypothesize that a third species, possibly ammonia, might be involved in the nucleation mechanism, which would explain the deviation between the bimolecular theory and measurements. *Nilsson and Kulmala* [1998] showed that atmospheric mixing processes such as entrainment might produce a substantial enhancement of the nucleation rate. Part of the discrepancy may also be caused by the fact that classical nucleation theory is based on thermodynamic bulk properties, which is not realistic for the very small critical clusters that can not be classified as being in the liquid phase [*Preining*, 1998].

[5] Although nucleation events are frequently observed in the atmosphere, there have been few attempts to derive nucleation rates from observations. *O'Dowd et al.* [1998]

0148-0227/02/2001JD000683$09.00

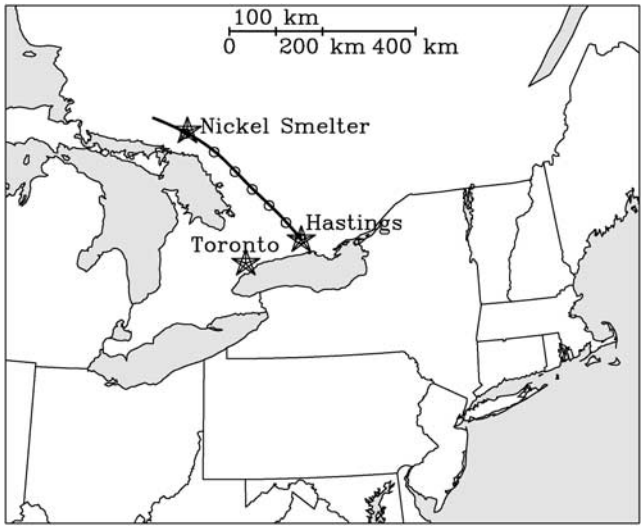

Figure 1. Map of Southern Ontario, Canada, showing Hastings (measurement site), Toronto Metropolitan Area, and the nickel smelter complex near Sudbury. Air mass back trajectory is for arrival of air mass in Hastings at 11:00 at 435 meters altitude. Dots indicate 2 hour intervals.

have made estimates of nucleation rates from temporal variations in ultrafine particle concentrations. However, their method does not account for the time required for the particles to grow to detectable size or for how coagulation or dilution may affect the concentration during this time. Recently, they have estimated the nucleation rate by employing an aerosol growth and dynamics model to match the aerosol size distributions, and infer what combination of precursor concentration and nucleation rate gave the best fit with the measurements [*O'Dowd et al.*, 1999]. *Weber et al.* [1995] estimate a "formation rate," defined as the rate at which particles grow past the small size range of 3–4 nm diameter. Although this size range is close to the assumed diameter of the critical cluster (1 nm), coagulation and dilution during the time required for growth alter the calculated value from the actual nucleation rate.

[6] In a spatially and temporally homogeneous situation the growth rate can be deduced from the time delay between the increase in precursor concentration and (ultra)fine particle number [*Weber et al.*, 1997]. If the location of the precursor source is known and constant in time, the inferred transport time to the measurement site can be used to determine the growth rate [*Weber et al.*, 1998; *O'Dowd et al.*, 1999], although dilution and coagulation would have influenced the size distribution during this time delay or during transport time, respectively. *Mäkelä et al.* [1997] and *Kulmala et al.* [1998b] estimate the growth rate from the evolution of the maximum particle number in the size distributions under homogeneous conditions. These ways of determining the growth rate are limited by the special conditions they require, and they provide an estimate of the growth rate only for a specific size and often averaged over longer time and larger size scales.

[7] Since our measurements indicate the presence of a plume, meaning no spatial or temporal homogeneity, we cannot deduce information on the growth from the observed time delay between SO_2 and nucleation mode particles. Instead, a quantitative method, following the same principle as used by *McMurry and Wilson* [1982], is developed to determine the growth rate from the evolution of the size distributions. By accounting for coagulation and dilution and by using a range of size intervals rather than a total number [i.e. *O'Dowd et al.*, 1998, 1999] or only one size interval [i.e. *Weber et al.*, 1995; *Mäkelä et al.*, 1997; *Kulmala et al.*, 1998b], we obtain more accuracy in determining both the atmospheric growth and nucleation rates [*Verheggen and Mozurkewich*, 1998, 2000].

[8] On the timescale of this nucleation event and especially on the timescale of two consecutive measurements, we assume that the history of the measured air mass has not changed. This means we can deduce growth rates from the change in the size distribution over time, although the experimental setup is not Lagrangian. We believe that this method can serve as a powerful tool to improve our understanding of nucleation by providing data on nucleation in the atmosphere that do not depend on the classical theory.

[9] We apply this method to a nucleation event that was observed in measurements performed as part of the Southern Ontario Oxidant Study (SONTOS) field campaign in Hastings, Ontario, Canada, in 1993. A burst in nucleation mode particles clearly correlated with, but lagged behind, a peak in SO_2 mixing ratio that reached 5 ppbv at ground level. To quantify the nucleation rate, the particle growth rate is obtained from the measured size distributions and is extrapolated backward to the time of formation. In principle, the method described here to determine the growth rate could also be used to determine the formation time. Since the growth rate for these small particles is independent of size, the measurements can provide the growth rate needed for extrapolation down to the critical cluster size. Consecutive measurements of the aerosol size distributions in a relatively homogeneous environment are all that is needed to determine the growth and nucleation rates. However, in this case study, the nucleation took place aloft under conditions that were different from those revealed by the ground level measurements. Therefore the method is supplemented by calculations of the rate of growth due to condensation of sulfuric acid and water. This is used to extrapolate the observed growth backward and to find the time of particle formation. The sulfuric acid concentrations are calculated using a one dimensional gas-phase model. Ground based measurements of H_2SO_4 would not have eliminated the need for model calculations of the H_2SO_4 concentrations aloft.

2. Observations

[10] The SONTOS field study was designed to examine photochemical oxidant formation at a rural site near Hastings, Canada, north of Lake Ontario (see Figure 1), during the summers of 1992 and 1993. A wide range of species involved in this process were measured; details are given by *Reid et al.* [1996, and references therein]. In 1993, aerosol size distributions were measured with a differential mobility analyzer (DMA, TSI model 3071) and condensation nucleus counter (CNC, TSI model 3020). There were a total of 17 size bins with midpoint diameters ranging from 11 to 457 nm; scans were completed at intervals of approximately eleven minutes. A Royco particle counter provided 6 size

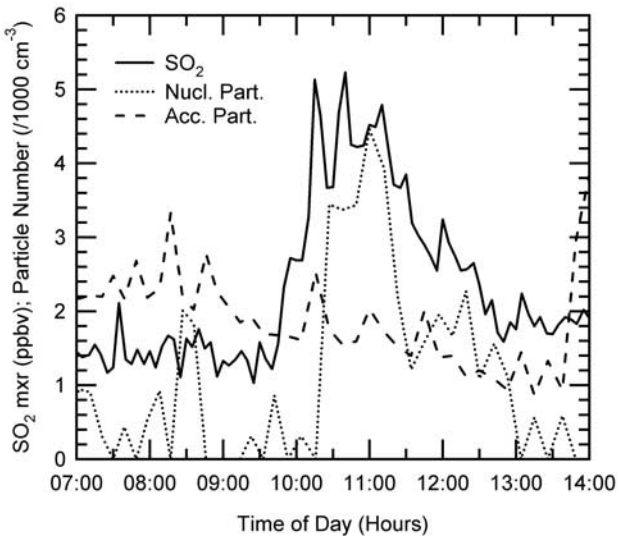

Figure 2. Arrival of the SO_2 plume at Hastings on 25 August 1993. The arrival of the SO_2 plume is followed by an increase in nucleation mode particle concentration, while the accumulation mode particle concentration is steadily decreasing over the same time period.

bins from 0.5 to 15.0 μm diameter. In addition, a second CNC (TSI model 3020) was used to measure total particle concentrations with a nominal lower diameter limit of 6 nm; these measurements were averaged over five minute intervals. Typically, the sum of concentrations over all DMA size bins was about 80% of the concentration measured by the CNC in spite of the fact that the two systems were carefully inter-calibrated in the laboratory. The noise in this ratio was larger than would be expected for a purely systematic error, and therefore the difference was attributed to particles with sizes between the lower diameter limits of the CNC (6 nm) and the DMA (10 nm). This additional "size bin" however was found to add more noise to the data rather than providing more information, so it was not incorporated in the analysis.

[11] During the SONTOS field experiment a burst of particle formation was observed on 25 August 1993. On this day, all measured gases (O_3, SO_2, NO, NO_2, CO, and hydrocarbons) were present at relatively low concentrations. This indicates that the air mass observed on that day was not strongly influenced by polluted air from Toronto. With the exception of SO_2 and nucleation mode aerosol particles, trace species concentrations were nearly constant on this day. Figure 2 shows that, beginning at 09:45 Eastern Daylight-saving Time, the SO_2 concentration increased from 1.5 to 5 ppbv in less than one hour. After a time delay of 30 min the number density of nucleation mode particles increased sharply. The time delay shows that these particles were not emitted simultaneously with the SO_2, but implies that they were formed recently by homogeneous nucleation. All other species remained at or near their initial low levels as typified by the O_3 and NO_x data in Figure 3. The levels of these species change after 8:25 due to the break-up of the nocturnal inversion. The relative humidity and temperature at the site are steadily decreasing and increasing, respectively. The CO concentration decreased from 200 to 150 ppbv while the total aerosol surface area varied between about 100 and 200 $\mu m^2\ cm^{-3}$ during this time.

[12] The air mass back trajectory indicates that the SO_2 was probably emitted before midnight by the nickel smelters near Sudbury, Ontario (approximately 400 km northwest of Hastings, see Figure 1). The back trajectory was calculated from three-dimensional wind fields generated by the MC2 model [*Benoit et al.*, 1997]. The MC2 model is a non-hydrostatic limited area model and was run for this day on a 2000 × 2000 km^2 domain at a horizontal resolution of approximately 21 km, driven by objectively analyzed meteorological fields provided by the Canadian Meteorological Centre (D. A. Plummer, personal communication, 2001). The trajectory shown in Figure 1 is for the air mass arriving at Hastings at 11:00 local time (which is the time that the maximum SO_2 concentration was observed) at an altitude of 435 meters above ground level, close to the assumed level of the plume. While the plume is mixing down through the growing boundary layer, the vertical wind shear is expected to cause the air mass to slightly divert from the path of the trajectory for approximately the latest hour. This is not accounted for in this analysis.

[13] We assume that the SO_2 plume traveled above the nocturnal inversion to the measurement site. The observation of the SO_2 plume at ground level follows the breakup of the nocturnal inversion. Similar behavior of these plumes has been observed previously [*Hoff and Gallant*, 1985]. Unfortunately there are no vertical soundings of the atmosphere available for this day, which evokes a high uncertainty in assessing the ambient boundary layer formation and thus in assessing the history of the air mass. However, a number of factors lead us to have confidence in our

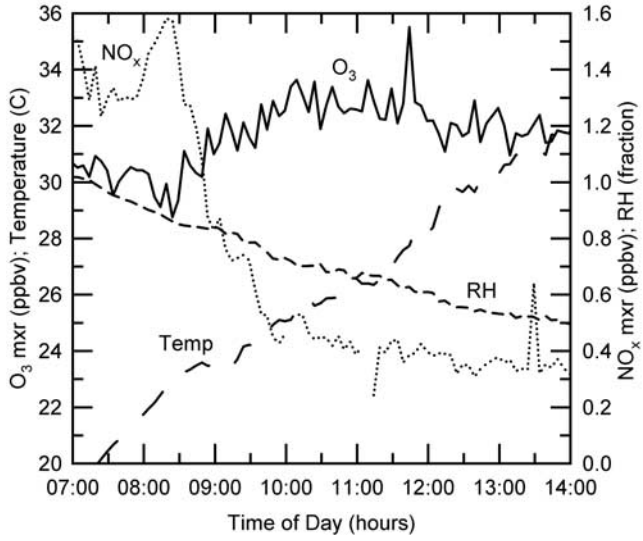

Figure 3. Time evolution of key quantities during the arrival of the plume. The O_3 and NO_x concentrations indicate the growth of the boundary layer starting at 8:25; their relatively low and constant values during the arrival of the SO_2 plume indicate that they were not at elevated concentrations in the plume. Temperature and relative humidity steadily increase and decrease, respectively, during the morning.

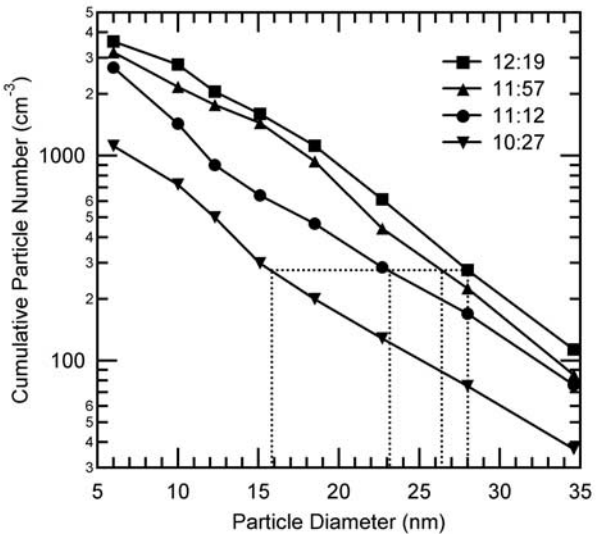

Figure 4. Cumulative size distribution of nucleation mode particles at consecutive times, corrected for dilution and coagulation. The horizontal line defines the growth of one cohort of particles; the intersections of this line with the distribution curves give the particle cohort diameters at the times the distributions were measured. The vertical dotted lines indicate this sequence of cohort diameters; the growth of the distribution is evident. For clarity, only four of the eleven size distributions from 10:27 to 12:20 are shown.

modeling of this process. These include the temporal change in measured key parameters such as wind speed and direction, ozone, nitrogen oxides, accumulation mode particles and carbon monoxide, the absence of strong local SO_2 sources, the air mass back trajectory, and the ability of the model to provide a reasonable simulation of the concentrations of the many different measured species including the SO_2 as it is mixed down. All of these support the assumed history of the air mass.

[14] The ground level SO_2 concentration (Figure 2) increases due to mixing of the plume downward when the nocturnal inversion is breaking up, and decreases due to mixing with clean upper level air as the boundary layer grows. If particle nucleation occurs aloft where the SO_2 concentration is highest, then the newly formed particles will be mixed in a similar manner. As a result, these newly formed particles will undergo substantial dilution before they are measured at ground level. This, as well as coagulation, is accounted for in the following analysis.

3. Determination of Growth Rate From Measured Size Distributions

[15] A number of processes cause the size distribution to change, the most important ones being growth (or shrinkage) by condensation (evaporation) of semi-volatile vapors and associated water, uptake or release of water by changing relative humidity, dilution, and coagulation. The first two of these processes affect the diameter and therefore define the growth rate, while the latter two affect the number density and can thereby mask the change in diameter. In the time interval that we use to deduce the growth rates (approximately 2 hours), we assume that the size distribution of nucleation mode particles is not significantly influenced by a change in air mass, but rather by those four processes. Here, the nucleation mode particles are defined as those between 10 and 43 nm diameter, which is the upper limit of the bin, centered on 38 nm, that usually contained the minimum between the nucleation and accumulation modes on this day.

[16] Figure 4 shows the cumulative distributions (number of particles larger than a certain diameter) of the nucleation mode particles measured at different times, corrected for dilution and coagulation with 12:19 as the reference time. Now consider a cohort of particles that were formed at the same time. Since they all grow at the same rate, the number of nucleation mode particles larger than this cohort changes only by dilution and coagulation. Once these processes are accounted for, the corrected number of particles larger than this cohort remains constant. Thus a horizontal line through the cumulative distributions in Figure 4 defines the growth rate for a cohort of particles. Starting out with the cumulative size distribution at a particular measurement time, horizontal interpolation gives the diameter of the same cohort at different times. Provided that the particle number is corrected for losses by coagulation and dilution, this gives us the growth rate in that time interval. By taking two consecutive measurements for the interpolation, errors due to the interpolation are minimized. The prerequisite of homogeneity need only be fulfilled at the timescale of two consecutive measurements, 11 min. We use this growth rate to calculate backward in time when the particles were formed.

[17] To calculate the nucleation rate, we ultimately need the number of particles that were formed. As the plume is mixed downward, the particle number in every cohort decreases due to dilution and coagulation. Therefore, these processes must be accounted for, in order to obtain both the growth rate and the number of nucleated particles.

[18] The number densities are corrected for dilution by using SO_2 as a tracer. This is reasonable since the critical nucleating species, H_2SO_4, is formed from SO_2, while removal of SO_2 by oxidation and dry deposition amounts to only a few percent on the timescale of this event. The correction for coagulation uses a time and particle size dependent adjustment factor, $f(a, t)$. The following equation is used to correct all values to a reference time taken as $t = t_R$:

$$\frac{N(i,t)}{N_C(i,t)} = \frac{[SO_2(t)]}{[SO_2(t_R)]} e^{f(a_i,t)} \quad (1)$$

where N is number density of particles in size bin i and a_i is the particle diameter in bin i. For calculating the growth rate, the choice of reference time is arbitrary. The growth rate is calculated from each pair of consecutive measurements, with the later time used as reference (t_R). The corrected particle number, $N_C(i, t)$, represents what the number of particles would have been if there were no decrease due to coagulation and dilution between the two measurement times. Because of this use of a sliding reference time, the analytical method is different in detail from the illustration in Figure 4 which used a constant reference time (12:19).

[19] The coagulation adjustment factor, $f(a, t)$, can be deduced by noting that, from the properties of total differentials,

$$\frac{df}{dt} = \left(\frac{\partial f}{\partial a}\right)_t \left(\frac{da}{dt}\right) + \left(\frac{\partial f}{\partial t}\right)_a \quad (2)$$

In equation (2), $\left(\frac{\partial f}{\partial t}\right)_a$ represents the change of f with respect to time for particles of diameter a. df/dt is the change in f for a particular group of particles (denoted here as a cohort) as they change in size and is given by

$$\frac{df}{dt} = -k_c(a, t) \quad (3)$$

where $k_c(a, t)$ is the pseudo-first order rate constant for removal of particles with diameter a by coagulation with accumulation mode particles.

[20] The coagulation scavenging rates were computed for each size bin at each time by using the equation of *Sceats* [1989] to obtain the second order coagulation rate constants for each pair of particle sizes. Then the pseudo-first order rate constant was obtained by summing the products of the second order rate constant and the measured particle concentration in the appropriate size bin, larger than the one for which k_c was being determined. For the relatively modest concentrations of nucleation mode particles observed here, coagulation between the nucleation mode and the accumulation mode is much faster than coagulation within the nucleation mode. Thus, the latter process was neglected in this analysis, which we will later show to be a valid assumption. As a result, the loss of nucleation mode particles can be treated as pseudo-first order.

[21] The effects of Van der Waals forces on the coagulation rate constant was included and the Hamaker constant was set to 1.0×10^{-19} J as an upper limit [*Chan and Mozurkewich*, 2001]. Particles with diameters of about 300 nm contributed the largest terms to the summation of the coagulation rates. Substituting equation (3) into equation (2) yields

$$\left(\frac{\partial f}{\partial t}\right)_a = -k_c(a, t) - \left(\frac{\partial f}{\partial a}\right)_t \left(\frac{da}{dt}\right) \quad (4)$$

This was solved numerically to obtain f as a function of a and t. The initial condition was taken to be $f(a, t_R) = 0$ for all particle sizes at the reference time (*cf* equation (1)). Since da/dt must be known in order to evaluate equation (4), an iterative procedure was required. The value of f proved rather insensitive to the growth rate, da/dt, resulting in rapid convergence. Then equation (1) was used to obtain $N_C(i, t)$, the particle number corrected for dilution and coagulation.

[22] As explained earlier, linear interpolation from the cumulative particle distribution at the reference time to the corrected distribution at the earlier time gives the growth rate of a particular cohort of particles. Over the time interval of interest (10:27–12:19) the average particle diameter growth rate plus or minus one standard error was found to be 4.2 ± 0.8 nm hr^{-1}.

[23] The recently nucleated particles were only measured at ground level from 10:27 onwards, since that is the time at which the SO_2 (and aerosol) plume was fully entrained. Before 10:27 the background aerosol was measured; at this time most of the newly formed particles were still aloft. Since the measurements only provide information on the nucleated particles after 10:27 and above 10 nm diameter, the observed growth indicated by the development of the cohort diameters needs to be extrapolated backward in time to reveal the time of particle formation and to calculate the nucleation rate. This is done using the modeled sulfuric acid concentration as described in the next section. The modeled growth is checked against the measured growth for times after 10:27.

4. Modeling the Sulfuric Acid

[24] A one-dimensional photochemical gas-phase diffusion model is used to calculate the H_2SO_4 concentration. These model-calculated H_2SO_4 concentrations are used to calculate the growth of newly formed particles, assuming condensation by H_2SO_4 vapour to be the main growth process. Full details about the model are given by *Plummer et al.* [1996]. The time evolution of the mixing ratio for the species within the model is governed by the one-dimensional form of the continuity equation. Fluxes into or out of the model, including emissions and dry deposition, are treated as part of the chemistry term.

[25] The height of the boundary layer is parameterized to give a diurnal profile as described in *Stull* [1988]. The value for the eddy diffusion coefficient K_z is dependent on time, t, and on height, z. The nocturnal inversion is set to 100 metres altitude with K_z fixed at 3.0×10^3 cm^2 s^{-1} within that layer. Above 100 metres K_z is set to 1.0×10^2 cm^2 s^{-1}. The behavior of the boundary layer during daytime is parameterized using the time-dependent function for K_z given by *Singh et al.* [1993]. An exponential height dependence is included. The well mixed boundary layer starts forming at 08:30, which compares well with the measurements (Figure 3), and reaches its maximum of 1650 metres at 13:00, with K_z reaching 1.0H10^6 cm^2 s^{-1} above 1000 metres. This produces good agreement with the observed diurnal pattern of measured species, including SO_2. The top of the model is in the free troposphere at 1850 meters. There are 22 vertical layers, with increasing resolution at lower altitudes.

[26] The temperature at the bottom grid point of the model is calculated by a radiative balance model. The decrease of temperature with height is assumed to occur at the dry adiabatic lapse rate (9.8 K km^{-1}) when the atmosphere is well mixed. The temperature profile before the boundary layer is fully developed simulates a nocturnal temperature inversion of 2 K at 100 meters altitude and a lapse rate of 6 K km^{-1}. The temperature measurements at ground-level are matched extremely well by the model simulation. Unfortunately no measurements of vertical profiles are available.

[27] The model includes the main species in tropospheric photochemistry, 85 in total, in 161 reactions. Gas phase H_2SO_4 is produced from the oxidation of SO_2 by the OH radical (K = 8.9×10^{-13} cm^3 molecule^{-1} s^{-1} [*DeMore et al.*, 1997]). Since the day in question was under a clear sky, no aqueous phase SO_2 oxidation reactions were included. Both condensation and dry deposition are loss processes for H_2SO_4. In this case dry deposition, set at

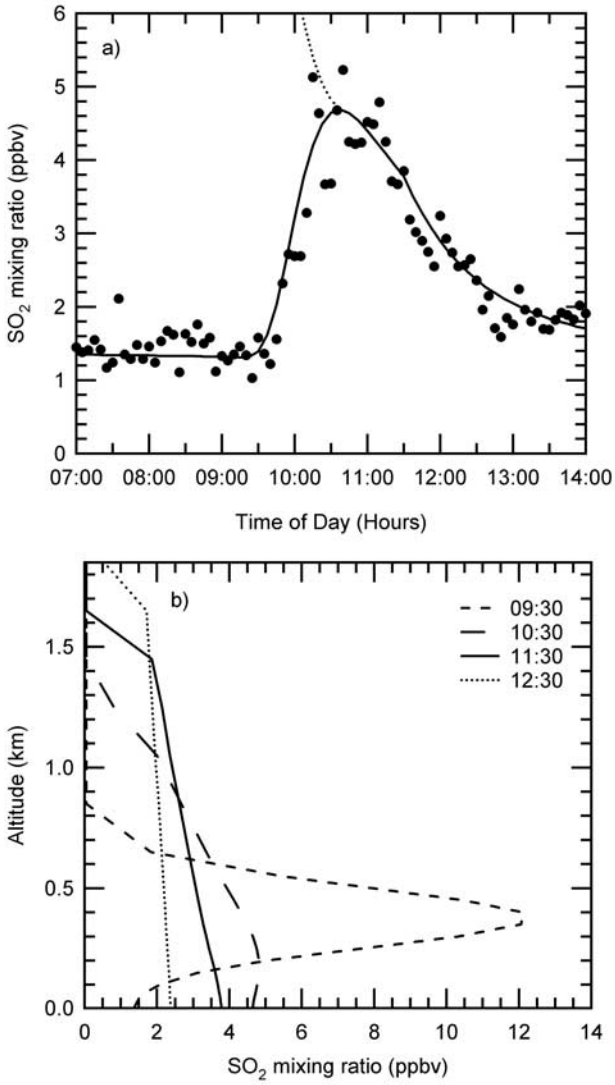

Figure 5. (a) Model simulation (lines) of diurnal profile of SO_2 mixing ratios at ground level (solid line) and at the level of the plume centre (dotted line), compared with measured mixing ratios (symbols). (b) Model simulation of the vertical profile of SO_2 at different times, showing the downward mixing of the plume. At 09:30, the plume has already been broadened by vertical mixing. The H_2SO_4 profiles are qualitatively very similar.

0.5 cm s^{-1}, was minor in comparison with condensation. It has been shown that measured H_2SO_4 concentrations agree well with calculated H_2SO_4 from the oxidation of SO_2 by OH when the mass accommodation coefficient is assumed to be in the range of 0.5 to 1 [*Eisele and Tanner*, 1993; *Weber et al.*, 1997]. The same steady state condition as they used is assumed in our calculations.

[28] The aerosol surface area was calculated from the measured size distribution and was used to simulate the condensation in the model as a sink for H_2SO_4. By adding the accumulation mode particle surface area as a conserved species in the model, only changing due to vertical mixing, a time and height dependence for the condensation was achieved. To simulate the measured pattern at ground level by vertical mixing, a lower initial accumulation mode particle surface area aloft was used. This favored nucleation, because the condensational sink for H_2SO_4 at the altitude of the plume was a factor of 1.5 weaker than at the surface, causing even higher vapour concentrations aloft. The (model-calculated) difference in relative humidity aloft and at ground level had a negligible effect on the surface area.

[29] The condensation rates were calculated using the equation of *Fuchs and Sutugin* [1970] with an accommodation coefficient, α, of 0.5. This is the lower limit of the range of likely values for this quantity [*Jefferson et al.*, 1997; *Pöschl et al.*, 1998]. Setting α to unity would increase the growth rate by about 25% since condensation on nucleation mode particles is more sensitive to this parameter than condensation on accumulation mode particles.

[30] The model was adjusted to match the observations to provide a realistic OH profile responsible for oxidizing the SO_2 to H_2SO_4. Sensitivity studies show that changes in concentration of various species, other than isoprene, within their range of measurement variation do not change the OH concentration by more than 15%. The simulated OH is primarily sensitive to isoprene for which only 5 daytime measurements are available. The simulation also serves as a good test for the assumed history of the air mass by examining the timing and magnitude of the SO_2 plume at ground level.

[31] The initial (0:00) concentration of SO_2 was chosen to be 1.5 ppbv up to 100 meters to match the measurements at ground level, 1.0 ppbv between 150 and 350 meters, increasing to 71 ppbv at 400 meters, then decreasing to 0.05 ppbv at 450 meters and above. Combined with the described formation of the boundary layer, this results in a good simulation of the SO_2 peak as measured at ground level. Figure 5a gives the measured and simulated diurnal profile of SO_2 at ground level. The increase of SO_2 is in good agreement with the measurements. In order to get good agreement for the decrease as well, a first order loss of 5.5% hr^{-1} is included after 11:30. The necessity of this extra loss rate is probably due to horizontal diffusion and transport processes not being dealt with by the 1-D model. Figure 5b shows how the SO_2 plume mixes down in time. The plume begins to disperse due to boundary layer growth just after 09:00.

[32] The H_2SO_4 concentration profiles are similar to the SO_2 profiles. The highest simulated H_2SO_4 concentration occurs at 400 meters, the height of the plume. This indicates that nucleation probably started aloft. Nucleation is also favored by lower aerosol surface area and lower temperature at higher altitudes.

[33] *Plummer et al.* [1996] found that an additional first order loss process of HO_2 was needed to prevent this model from being overactive in producing O_3 and peroxy radicals. In our model-runs we assumed that HO_2 was lost on the particles with a reaction probability of unity. Smaller values of the reaction probability resulted in higher OH concentrations and larger modeled growth rates. The HO_2 loss rate was calculated in the same way as condensation of H_2SO_4. The resulting pseudo-first order loss rates for HO_2 were much smaller than the loss rate assumed by *Plummer et al.* in spite of the particle number concentrations being similar on both days. They did not calculate the loss rate from the aerosol distribution, but instead used a solely empirical parameter to suppress the peroxy radical concentration. Unfortunately, no particle size distributions are available

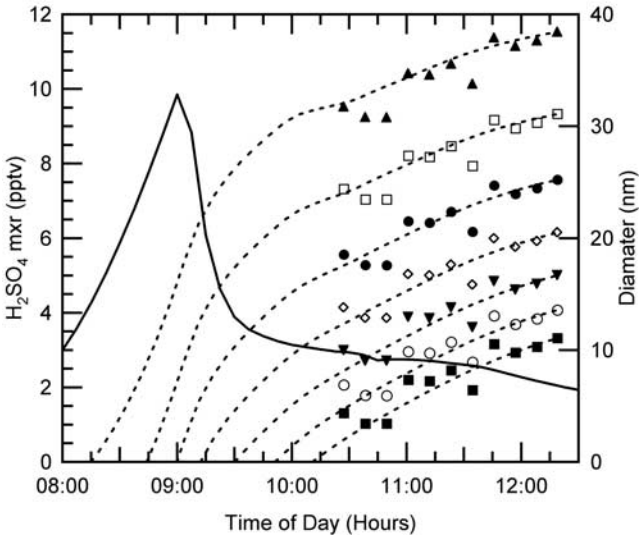

Figure 6. Cohort diameter versus time extrapolated to indicate the particle formation time. Symbols are determined from the corrected size distributions from 10:27 through 12:20 as illustrated in Figure 4. The dotted lines are particle growth curves obtained from the modeled H_2SO_4 concentrations. They are offset vertically to match the measurements as closely as possible. The backward extrapolation of the growth curves provides the particle formation time. The solid line is the modeled H_2SO_4 mixing ratio at the centre of the plume; it declines after 09:00 due to vertical mixing of the SO_2 plume through the growing boundary layer.

for the day analyzed by *Plummer et al.*, so a direct comparison is not possible. The additional HO_2 loss affects both the magnitude and the diurnal profile of the OH concentration.

5. Determination of Growth Rate From Model Calculated H_2SO_4

[34] The small particles that are observed at ground level were probably formed aloft. When the boundary layer started to form, these were mixed downward concurrent with the SO_2. At the same time, they grew by condensation of H_2SO_4. Most nucleation would have occurred where H_2SO_4 was at its maximum, which was at nearly the same altitude as the SO_2 maximum. Since the particles were mixed along with the SO_2, the largest part of them would have continued to be near the SO_2 maximum. Therefore, the H_2SO_4 concentration at the altitude where the SO_2 was at its maximum, was used to simulate the particle growth. This provides an upper limit for the growth, since a fraction of the observed particles would have grown under a sub-maximum H_2SO_4 regime. As a result, we might expect the calculated time of formation to be somewhat later (that is, nearer to the time of measurement) than the actual time of formation.

[35] To obtain the time of formation, the effect of water vapour condensing on or evaporating from the particle must also be considered, since this affects the particle size. Condensation of other species is assumed to be negligible, because of the extremely high SO_2 concentrations and relatively low levels of VOCs. Assuming the particle consists mainly of H_2SO_4 and H_2O, the particle volume can be written as

$$V = \frac{m_{H_2SO_4}}{w\rho} \tag{5}$$

where $m_{H_2SO_4}$ and w are the mass and weight fraction of sulfuric acid in the particle, and ρ is the particle density. The values of w and ρ are dependent on the ambient temperature and relative humidity, and are interpolated from the tables in *Gmitro and Vermeulen* [1964] and *Perry and Chilton* [1978]. A change in relative humidity affects w and ρ but not $m_{H_2SO_4}$, so the ratio of volumes at two consecutive measurement times, due to a change in relative humidity, is given by

$$\frac{V_1}{V_2} = \frac{w_2\rho_2}{w_1\rho_1} = \frac{a_1^3}{a_2^3} \tag{6}$$

where the subscripts denote the values at the two different measurement times, and a is particle diameter.

[36] Differentiating equation (5) with respect to time, and substituting the equation for condensational growth [*Fuchs and Sutugin*, 1970] gives for the diameter growth rate, in the limit of infinite Knudsen number,

$$\begin{aligned}\frac{da}{dt} &= \frac{2\alpha\, c[H_2SO_4]M_{H_2SO_4}}{4\rho\, w\, N_A} - \frac{a}{3}\frac{d\ln(\rho w)}{dt} \\ &= (0.253)\frac{X_{H_2SO_4}}{\rho w} - \frac{a}{3}\frac{d\ln(\rho w)}{dt}\end{aligned} \tag{7}$$

where α is the mass accommodation coefficient (set to 0.5), c is the mean molecular speed of H_2SO_4 molecules, $M_{H_2SO_4}$ is the molecular weight of H_2SO_4 and $X_{H_2SO_4}$ is the volume mixing ratio of H_2SO_4. The constant 0.253 has units of m s^{-1} g cm^{-3} and is evaluated at an air density of 2.45×10^{19} molecules cm^{-3} (10^5 Pa, 295 K). The first part of this equation describes the growth by condensation of sulfuric acid ($m_{H_2SO_4}$ changing in time). The second part describes the growth (or shrinkage) by uptake (or release) of water (ρ and w changing in time); its (size-averaged) contribution to the growth rate is -0.8 nm h^{-1} (i.e. shrinkage) over the time period of interest (10:27–12:19).

[37] The growth rates calculated using equation (7) were larger than the growth rates based on measurements for the time period after the plume had reached the ground. The model-calculated growth rate can be slightly reduced by assuming a reaction of HO_2 with the particles and by reducing the value assumed for the H_2SO_4 mass accommodation coefficient. Even assuming a HO_2 reaction probability of unity and a H_2SO_4 mass accommodation coefficient of 0.5 gave growth rates that were more than double the measured rates. This is not too surprising since this photochemical model has been shown before to be over-reactive in terms of the radical budget relative to observations [*Plummer et al.*, 1996]. Since we trust the measured growth more than the modeled growth, all OH and consequently H_2SO_4 concentrations produced by the model were reduced by a factor of 2.5. The resulting growth curves, calculated using equation (7), are shown in Figure 6. These agree well with the growth determined from the measured size distributions.

[38] The growth rate of 4.2 nm hr^{-1} is higher than values reported by *Weber et al.* [1997], but similar to values found by *Mäkelä et al.* [1997], *Kulmala et al.* [1998b] and *Weber et al.* [1998]. The fact that our growth rates are larger than found by *Weber et al.* [1997] is due to the higher SO_2 and H_2SO_4 concentrations encountered in our study, while biogenics are expected to dominate the growth rate in their 1998 study and in the forested environment in the studies by *Mäkelä et al.* [1997] and *Kulmala et al.* [1998b]. It is interesting to note that *Weber et al.* [1997, 1998] found the observed growth to be higher than the growth calculated from the condensation of H_2SO_4; this is opposite of our results. For the calculation of the growth they used measured H_2SO_4, while we use calculated values. *Eisele and Tanner* [1993] and *Weber et al.* [1997] have shown that their calculated and measured concentrations agree well.

[39] The large discrepancy between the growth rates caused *Weber et al*. to conclude that another mechanism besides condensation of H_2SO_4 was contributing to the growth. Modeling studies indicate that condensation of other species has the potential to considerably enhance the binary growth rate [*Kerminen et al.*, 1997]. In our case study, the observed isoprene concentration at 12 noon was 0.4 ppbv. No measurements of pinenes were available. Quantitative assessment of the role of biogenic emissions falls beyond the scope of this paper, but they are expected to have a minor influence on the observed growth rate as compared to H_2SO_4. In both cases described by *Weber et al.* [1997, 1998], the probability of other species contributing significantly to the growth rate is much higher. This increases their ratio of the observed growth rate over the growth rate calculated from the condensation of H_2SO_4 and H_2O only. A larger contribution of biogenic or other species to the growth rate might be a (partial) explanation for the difference in discrepancy between the cases presented by *Weber et al.* [1997, 1998] and by us, as well as the overreactivity of the 1D-model used here.

[40] We neglect the effect of other condensing species and attribute the difference between the calculated and measured growth rates to uncertainty in the model calculated OH concentrations.

6. Determination of the Nucleation Rate

[41] Figure 6 shows several growth curves starting at various times, assuming that condensation of H_2SO_4 and H_2O is the only growth process. For such small particles, growth by condensation of H_2SO_4 should be nearly independent of particle size. Accordingly, the particles that formed between 09:00 and 09:12 reached diameters between 12.5 and 17.5 nm at 10:27. The number of nucleated particles is obtained by correcting the particle number, measured at 10:27 between 12.5 and 17.5 nm diameter, for losses due to dilution and coagulation that have occurred since they formed. Dividing the number of nucleated particles by the time interval in which they were formed (12 min in this example) gives the nucleation rate. The diameter range is equal to the formation time interval multiplied by the average growth rate during that time. Thus, the nucleation rate can also be obtained by multiplying the concentration per unit size interval by the growth rate, both evaluated at the time of formation. To obtain the diameter range at the time of measurement, the effect of changing relative humidity must be accounted for.

[42] To carry out this calculation, we let $n(a, t)$ be the measured size distribution function (concentration per unit size interval) at time t; this is just the concentration of particles in a bin divided by the width of the bin. Let $t = t_N$ be the time of nucleation, a_N the diameter of a recently nucleated particle (i.e., the critical cluster), and $(da/dt)_{tN}$ the growth rate at the time of nucleation. The nucleation rate is simply the rate at which particles grow past the critical cluster diameter, a_N, and is given by

$$J(t_N) = n(a_N, t_N) \left(\frac{da}{dt}\right)_{t_N} \tag{8}$$

This formula can be readily obtained by integrating the General Dynamic Equation (GDE) from a_N to infinity and evaluating the contribution of the growth term to the evolution of the total particle concentration. The other significant processes that are represented by the GDE are incorporated in the analysis by the same method as was used to account for these processes in determining the growth rate. Clearly, $n(a_N, t_N)$ is not directly measurable, but it can be obtained from the measured size distribution, $n(a, t)$ at a later time, t via

$$n(a_N, t_N) = n(a, t) \frac{[SO_2(t_N)]}{[SO_2(t)]} \exp\left(\int_{t_N}^{t} k_c(a', t')\, dt'\right)\left(\frac{w(t_N)\rho(t_N)}{w(t)\rho(t)}\right)^{1/3} \tag{9}$$

where a' is the diameter at time t' of the cohort of particles that were formed at time t_N. Substituting equation (9) into equation (8) allows us to account for the effects of dilution, coagulation, and particle size changes due to changes in relative humidity during the time that elapsed between particle formation and measurement.

[43] Equation (9) is a straightforward adoption of equation (1) with $f(a, t)$ computed from equation (3). Equation (3) is used instead of equation (4) since here we are accounting for the effect of coagulation on the concentration of a cohort of particles as they grow. In equation (8) the distribution function must be used, while equations (1) and (9) could be applied to either the distribution function or to the concentration in each size interval. Basically, $n(a_N, t_N)$ is the measured size distribution function corrected for the losses integrated over the time interval between formation and measurement. It is the number of nucleated particles per unit size interval.

[44] Equations (8) and (9) were applied to each measured size bin in the nucleation mode (up to 43 nm diameter) for each measurement time from 10:27 to 12:19. For each bin, the model calculated growth rates were used to determine the time of formation for particles in that bin. This is because the ground level measurements can only be used to determine the growth after 10:27. When applying equation (9) before 10:27, the SO_2 concentration at the height at which it was at a maximum (i.e., the height at which the growth was calculated) was used.

[45] In evaluating equation (9), the coagulation rate varies with time as a result of changes in the concentration of

accumulation mode particles and because of the changing particle size for which the coagulation rate was calculated. Using the coagulation rates calculated as described above, it was found that k_c is proportional to $a^{-1.7}$; this was used to provide a continuous function for the size dependence of the coagulation rate. Since the coagulation rate diverges as the particle diameter goes to zero, it was necessary to pick a definite value for a_N. A diameter of 1.0 nm was chosen; this is the same as the value used by *Weber et al.* [1997]. Increasing or decreasing this diameter by a factor of two only changes the formation times by about two minutes. However, doubling this diameter reduces the calculated nucleation rates by about a factor of three; halving it increases the nucleation rates by an order of magnitude. This is because these very small particles are rapidly scavenged by coagulation.

[46] Because of the initially high concentration of very small particles, the effect of coagulation within the nucleation mode must be evaluated as a potential loss and growth process. This is done by comparing the rate of production of new particles (i.e. the nucleation rate) to the rate of removal by within-mode coagulation (R_C). The latter can be written as

$$R_C = k_c(II)(N_n)^2 \tag{10}$$

where N_n is the number of particles with diameter between 1 and 10 nm, and $k_c(II)$ is the second order rate constant for coagulation of monodisperse aerosols. Note that $k_c(II)$ denotes the second order rate constant for coagulation, while k_c stands for the pseudo-first order rate constant. To calculate the maximum loss rate, N_n is evaluated for the time that the calculated nucleation rate is highest, and $k_c(II)$ is set to 2×10^{-9} cm^3 s^{-1} as an upper limit [*Seinfeld and Pandis*, 1998].

[47] If the main loss process is coagulation scavenging by the accumulation mode, then the concentration of particles in any cohort decreases exponentially as the cohort grows. Therefore, since $n(a)$ represents cohorts of increasing age as size increases, we expect $n(a)$ to be a roughly exponential function for the nucleation mode, while nucleation is occurring. Thus, N_n can be expressed as

$$N_n = \int_1^{10} c\, e^{(-b \bullet a)} da = \frac{n(1) - n(10)}{b} \tag{11}$$

where c and b are constants, and a is diameter. The size distribution functions $n(1)$ and $n(10)$ are obtained from equation (9) and directly from the measurements, respectively. While the constant, c, does not need to be known, the scaling factor, b, can be obtained by simple rearrangement of the exponential function:

$$\ln\left(\frac{n(1)}{n(10)}\right) = b \bullet \Delta a = b \bullet (9\ nm) \tag{12}$$

[48] Via this procedure, the maximum N_n is found to be approximately 2×10^4 particles cm^{-3}, giving a loss rate of about 10% of the calculated nucleation rate. The time constant for within-mode coagulation, $\tau = N_n/(dN_n/dt)$, is 7 hours, considerably longer than the time needed to grow from 1 to 10 nm diameter (less than 1 hour). Taking into account the large uncertainties in calculating the nucleation rate, and the fact that this estimate is a maximum loss rate, it is concluded that neglecting within-mode coagulation is a valid assumption for the present calculations. By neglecting the growth of very small particles due to within-mode coagulation, the growth rate is slightly underestimated. However, the maximum reduction of 10% in number density produces an increase in average diameter of only 3%. Since this is a maximum, we can also neglect the effect of coagulation on the growth rate.

[49] In using equation (9) to determine the critical cluster concentration, there are three factors that contribute. The correction factors for dilution range from 1.9 to 22 (median value 11.5). The correction factors for coagulation range from 2.5 to 26 (median value 3.8). The correction factors for relative humidity range from 0.83 to 0.91 (median value 0.87). Obviously, the uncertainty in the latter, dependent on the modeling of relative humidity aloft and estimated at 10%, does not have a large effect on the nucleation rates obtained. The other two factors increase as the particle size at the time of measurement increases; this is because these particles are ''older'' and have had more time to be affected by these processes.

[50] The accuracy of the dilution correction depends on both the magnitude and time dependence of the modeled SO_2 plume. A reasonable match to the ground-based measurements requires peak SO_2 concentrations within 20% of those assumed; this corresponds to the maximum uncertainty in the dilution correction, which only applies to formation times of 9:00 or earlier.

[51] The coagulation correction depends on two factors: the assumed accumulation mode size distribution aloft and the calculated coagulation rate constants. Since the accumulation mode particles do not change much during the growing of the boundary layer, their size distribution can not have been much different aloft. The coagulation rate constants are based on a widely accepted theory. A reasonable estimate of the uncertainty in k_c is 10%, which leads to uncertainties of 9 to 32% in the correction factor.

[52] The large coagulation correction factors are due to the rapid removal of very small particles by coagulation scavenging. As a result, only a fraction of newly formed particles grow to a detectable size. We expect that this will be a general result for moderately polluted conditions where the total surface area of the accumulation mode particles is relatively large. The uncertainty in nucleation rates due to noise in the measurements, propagated via the determination of growth rates, will be discussed below.

[53] The calculated nucleation rates as a function of time are shown in Figure 7a. To reduce the noise, groups of seven successive points are averaged; error bars are one standard error of the mean. The noise may be due in part to real variation in the nucleation rate, but it is at least as likely due to uncertainties in both the calculations and the measurements. The calculated nucleation rates are in the range of 5 to 40 particles cm^{-3} s^{-1}. The H_2SO_4 mixing ratio and relative humidity in the plume, as calculated from the model, are shown in Figure 7a as well. Figure 7b shows the (averaged) nucleation rates for three different cases: By using the average growth rate (4.2 nm h^{-1}) and by using the high and low estimate (average plus or minus one standard error,

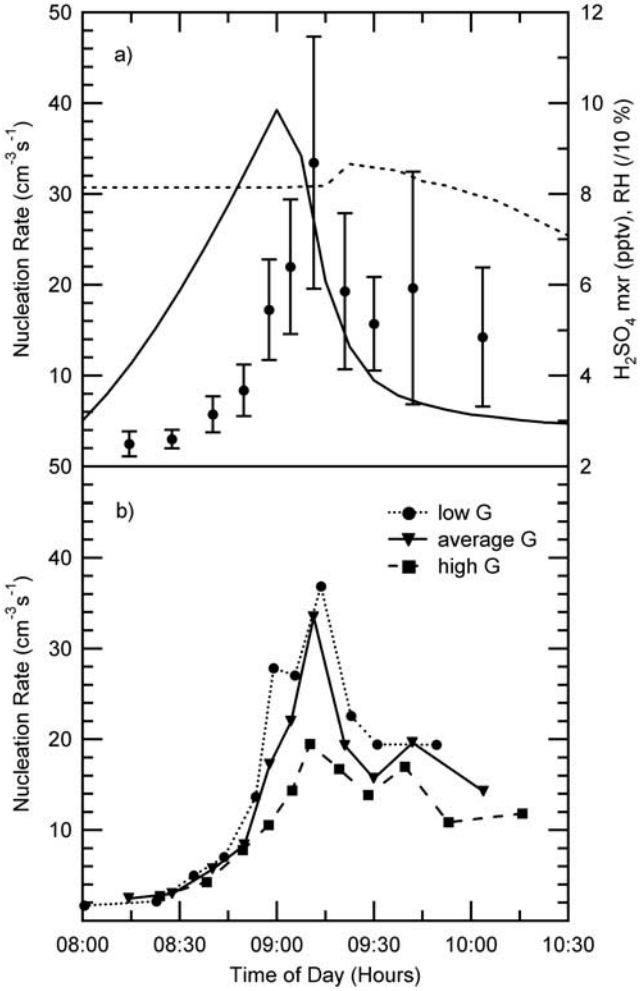

Figure 7. (a) Modeled RH (dotted line) and H_2SO_4 mixing ratios (solid line) and calculated nucleation rates (symbols) as a function of time, at the centre of the plume while it is mixing down. The estimates for the nucleation rate have been averaged over seven successive points; error bars are standard errors. (b) The sensitivity of the calculated nucleation rate to the variation in the growth rate (G), by employing the average growth rate deduced from the measurements, and the high and low estimate (average plus or minus one standard error).

0.8 nm h^{-1}) of the growth rate. It can be seen that in the case with lower estimated growth rate (lower H_2SO_4 concentration) the calculated nucleation rates are found to be higher. This is because a smaller growth rate means more time has passed between particle formation and measurement, resulting in greater losses by coagulation and dilution. Mathematically, $n(a_N, t_N)$ has increased to a greater extent than $(da/dt)_{tN}$ has decreased, compared with the case of average growth, resulting in a higher value for $J(t_N)$ in equation (8). This does not imply a cause-effect relationship; it is simply due to the propagation of the error in the growth rate.

[54] In Figure 7a it can be seen that the maximum nucleation rate occurs about ten minutes after the maximum H_2SO_4 mixing ratio. It is unlikely that the calculated formation times are sufficiently accurate for this difference to be significant.

[55] Figure 7a also shows that the nucleation rate rises rapidly as the H_2SO_4 concentration rises; this is to be expected. However, after the peak near 09:15, the nucleation rate seems to decrease slower than the H_2SO_4 concentration does. To understand this we must recognize that the plume starts to be entrained into the growing boundary layer at about 09:00. Before this time, the nucleation is taking place under fairly homogeneous conditions within the plume. After this time, as mixing occurs, there are likely to be substantial, highly localized variations in concentrations that are not reproduced by the model. *Nilsson and Kulmala* [1998] have shown that this type of mixing has the potential to substantially enhance the binary nucleation rate. This effect could explain the higher nucleation rates found after 09:00 compared to those found before 09:00. Another contributing effect could be the presence of an additional source of condensable material closer to the ground (i.e. after the plume starts mixing down at 9:00), such as the oxidation products of biogenic organic compounds. Both the emissions and the oxidation rate of biogenics increase as temperature and sunlight intensity increase.

[56] It is interesting to compare our results with the predictions of nucleation theory. The theory provides an estimate of the critical H_2SO_4 concentration, that is, the concentration required to obtain a nucleation rate of 1 cm^{-3} s^{-1}. Since the nucleation rate is expected to vary in a highly non-linear manner as the H_2SO_4 concentration varies, we should expect that the rates observed here should require only a slight excess over the critical concentration. For the conditions at 09:00, the parameterization of *Kulmala et al.* [1998a] gives critical H_2SO_4 mixing ratios of 121 pptv at ground level (T = 296.6 K, RH = 0.83) and 101 pptv at 400 meters (T = 294.5 K, RH = 0.81), the altitude of the plume. The latter value is still a factor of ten higher than our maximum calculated mixing ratio. In contrast, the parameterization of *Kerminen and Wexler* [1996] gives critical sulfuric acid mixing ratios of 16 pptv (ground level) and 13 pptv (400 meters), which are slightly higher, but comparable to the mixing ratios inferred here. However, even this parameterization implies that no nucleation should have occurred, since these mixing ratios were not reached.

7. Conclusions

[57] We have developed a method to systematically quantify particle growth and nucleation from measured size distributions. The large discrepancies between nucleation theory and aerosol measurements clearly show a need for such an empirically based determination. We believe the method described here has the potential to be applied to relatively widespread situations, thereby offering the possibility of acquiring an observationally derived data set for nucleation rates in the atmosphere. Application of this method to other data sets and comparison with nucleation theory could provide more insight in the quantitative relation between the nucleation rate and environmental factors such as precursor concentration, temperature, and relative humidity.

[58] Several of the conditions favorable for nucleation as identified by *Mäkelä et al.* [1997] are similar to the conditions observed in our case: sunny and a large increase in temperature and decrease in relative humidity from morning to afternoon. Vertical transport of air masses was

an important factor to trigger the onset of nucleation in this study. However, substantial nucleation occurred in spite of a relatively large aerosol surface area of 100 to 200 $\mu m^2 cm^{-3}$. Apparently, this ''obstacle'' was overcome by the very high H_2SO_4 concentrations encountered.

[59] The method employed here allowed us to determine both the times at which particle formation occurred and the nucleation rate. The maximum nucleation rate coincided reasonably well with the maximum in the H_2SO_4 concentration. However, the nucleation rates of 5 to 40 particles cm^{-3} s^{-1} for H_2SO_4 mixing ratios of 3 to 10 pptv are larger than expected from parameterizations of the nucleation process.

[60] The assumed history of the air mass, which dictates the conditions under which H_2SO_4 is formed, is associated with a certain degree of uncertainty, although it is supported by strong evidence. A major source of uncertainty in this study is the model calculated H_2SO_4 profile; in order to get modeled growth rates that agree with those inferred from the measured distributions, we had to artificially reduce the OH mixing ratio by a factor of 2.5. This implies that the model was over-reactive with respect to radical formation and cycling. The fact that the maximum nucleation rate was calculated to occur at approximately the same time as the H_2SO_4 concentration was at its maximum, indicates that the model did not produce serious systematic errors in the H_2SO_4 profile. This is because such errors would have substantially shifted the calculated time of particle formation away from the maximum in H_2SO_4 concentration.

[61] The use of a model is not essential to the method described here; it was required in this case only because the ground level measurements could not be directly applied to the conditions under which nucleation occurred aloft. In principle, measurements of consecutive aerosol size distributions are all that is needed to obtain both the growth and nucleation rates. Future experiments may be able to reduce errors associated with the use of a model by making measurements under Lagrangian conditions. In that case there is no need to calculate the growth rate from either modeled or measured H_2SO_4, since it could be determined directly from the measurements and extrapolated down to the critical cluster size.

[62] Another source of uncertainty is that the size distribution measurements were rather noisy for the purpose of the growth measurements. Finally the method itself involves calculations of dilution and coagulation that are subject to uncertainty. In particular, the magnitude of the correction for coagulation scavenging is sensitive to the assumed critical cluster size. The overall uncertainty in the calculated nucleation rate is estimated to be a factor of two to three. Thus, this method could be a valuable tool for quantifying particle growth and nucleation rates from measured size distributions.

[63] **Acknowledgments.** We thank D. A. Plummer for assistance with the model and back trajectory and D. Sills, P. Taylor, and D. R. Hastie for helpful discussions. This work was supported by a grant from the Atmospheric Environment Service of Environment Canada and by a grant from the VSB Foundation Netherlands.

References

Andronache, C., W. L. Chameides, D. D. Davis, B. E. Anderson, R. F. Pueschel, A. R. Bandy, D. C. Thornton, R. W. Talbot, P. Kasibhatla, and C. S. Kiang, Gas-to-particle conversion of tropospheric sulfur as estimated from observations in the western North Pacific during PEM-West B, *J. Geophys. Res.*, *102*, 28,511–28,538, 1997.

Benoit, R., M. Desgagné, P. Pellerin, S. Pellerin, Y. Chartier, and S. Desjardins, The Canadian MC2: A semi-Lagrangian, semi-implicit wideband atmospheric model suited for finescale process studies and simulation, *Mon. Weather Rev.*, *125*, 2382–2415, 1997.

Chan, T. W., and M. Mozurkewich, Measurement of the coagulation rate constants for sulfuric acid particles as a function of particle size, *J. Aerosol Sci.*, *32*, 321–339, 2001.

DeMore, W. B., C. J. Howard, S. P. Sander, A. R. Ravishankara, D. M. Golden, C. E. Kolb, R. F. Hampson, M. J. Molina, and M. J. Kurylo, Chemical kinetics and photochemical data for use in stratospheric modeling, *JPL Publication 97-4*, NASA, Pasadena, Calif., 1997.

Eisele, F. L., and D. J. Tanner, Measurement of the gas phase concentration of H_2SO_4 and methane sulfonic acid and estimates of H_2SO_4 production and loss in the atmosphere, *J. Geophys. Res.*, *98*, 9001–9010, 1993.

Fuchs, N. A., and A. G. Sutugin, *Highly Dispersed Aerosols*, Ann Arbor Sci., Ann Arbor, Mich., 1970.

Gmitro, J. I., and T. Vermeulen, Vapor-liquid equilibria for aqueous sulfuric acid, *Amer. Inst. Chem. Eng. J.*, *10*, 740–746, 1964.

Hoff, R. M., and A. J. Gallant, The use of an available SO_2 tracer during the 1983 CAPTEX experiment, *Atmos. Environ.*, *19*, 1573–1575, 1985.

Intergovernmental Panel on Climate Change (IPCC), Radiative forcing of climate change, *Climate Change 1994*, edited by J. T. Houghton, L. G. Meira Filho, J. Bruce, H. Lee, B. A. Callander, E. Haites, N. Harris, and K. Maskell, 231 pp., Cambridge Univ. Press, New York, 1995.

Jefferson, F. L., Eisele, P. J. Ziemann, R. J. Weber, J. J. Marti, and P. H. McMurry, Measurements of the H_2SO_4 mass accommodation coefficient onto polydisperse aerosol, *J. Geophys. Res.*, *102*, 19,021–19,028, 1997.

Kerminen, V.-M., and A. S. Wexler, The occurrence of sulfuric acid-water nucleation in plumes: Urban environment, *Tellus, Ser. B*, *48B*, 65–82, 1996.

Kerminen, V.-M., A. S. Wexler, and S. Potukuchi, Growth of freshly nucleated particles in the troposphere: Roles of NH_3, H_2SO_4, HNO_3, and HCL, *J. Geophys. Res.*, *102*, 3715–3724, 1997.

Kulmala, M., and A. Laaksonen, Binary nucleation of water-sulfuric acid system: Comparison of classical theories with different H_2SO_4 saturation vapor pressures, *J. Chem. Phys.*, *93*, 696–701, 1990.

Kulmala, M., A. Laaksonen, and L. Pirjola, Parameterizations for sulfuric acid/water nucleation rates, *J. Geophys. Res.*, *103*, 8301–8307, 1998a.

Kulmala, M., A. Toivonen, J. M. Mäkelä, and A. Laaksonen, Analysis of the growth of nucleation mode particles observed in Boreal forest, *Tellus*, *50B*, 449–462, 1998b.

Leaitch, W. R., G. A. Isaac, J. W. Strapp, C. M. Banic, and H. A. Wiebe, The relationship between cloud droplet number concentrations and anthropogenic pollution: Observations and climatic implications, *J. Geophys. Res.*, *97*, 2463–2474, 1992.

Leaitch, W. R., C. M. Banic, G. A. Isaac, M. D. Couture, P. S. K. Liu, I. Gultepe, and S.-M. Li, Physical and chemical observations in marine stratus during the 1993 North Atlantic Regional Experiment: Factors controlling cloud number droplet number concentrations, *J. Geophys. Res.*, *101*, 29,123–29,135, 1996.

Leaitch, W. R., J. W. Bottenheim, T. A. Biesenthal, S.-M. Li, P. S. K. Liu, K. Asalien, H. Dryfhout-Clark, and F. Hopper, A case study of gas-to-particle conversion in an eastern Canadian forest, *J. Geophys. Res.*, *104*, 8095–8111, 1999.

Mäkelä, J. M., P. Aalto, V. Jokinen, T. Pohja, A. Nissinen, S. Palmroth, T. Markkanen, K. Seitsonen, H. Lihavainen, and M. Kulmala, Observations of ultrafine aerosol particle formation and growth in boreal forest, *Geophys. Res. Lett.*, *24*, 1219–1222, 1997.

Nemesure, S., R. Wagener, and S. E. Schwartz, Direct shortwave forcing of climate by the anthropogenic sulfate aerosol: Sensitivity to particle size, composition, and relative humidity, *J. Geophys. Res.*, *100*, 26,105–26,116, 1995.

Nilsson, E. D., and M. Kulmala, The potential for atmospheric mixing processes to enhance the binary nucleation rate, *J. Geophys. Res.*, *103*, 1381–1389, 1998.

O'Dowd, C. D., M. Geever, M. K. Hill, M. H. Smith, and S. G. Jennings, New particle formation: Nucleation rates and spatial scales in the clean marine coastal environment, *Geophys. Res. Lett.*, *25*, 1661–1664, 1998.

O'Dowd, C. D., G. McFiggans, D. J. Creasey, L. Pirjola, C. Hoell, M. H. Smith, B. J. Allan, J. M. C. Plane, D. E. Heard, J. D. Lee, M. J. Pilling, and M. Kulmala, On the photochemical production of new particles in the coastal boundary layer, *Geophys. Res. Lett.*, *26*, 1707–1710, 1999.

Perry, R. H., and C. H. Chilton, *Chemical Engineers' Handbook*, 5th ed., McGraw-Hill, New York, 1978.

Pilinis, C., S. N. Pandis, and J. H. Seinfeld, Sensitivity of direct climate forcing by atmospheric aerosols to aerosol size and composition, *J. Geophys. Res.*, *100*, 18,739–18,756, 1995.

Plummer, D. A., J. C. McConnell, P. B. Shepson, D. R. Hastie, and H. Niki, Modeling of ozone formation at a rural site in Southern Ontario, *Atmos. Environ.*, *30*, 2195–2217, 1996.

Pöschl, U., M. Canagaratna, J. T. Jayne, L. T. Molina, D. R. Worsnop, C. E. Kolb, and M. J. Molina, Mass accommodation coefficient of H_2SO_4 vapor on aqueous sulfuric acid surfaces and gaseous diffusion coefficient of H_2SO_4 in N_2/H_2O, *J. Phys. Chem.*, *102*, 10,082–10,089, 1998.

Preining, O., The physical nature of very, very small particles and its impact on their behaviour, *J. Aerosol Sci.*, *29*, 481–495, 1998.

Reid, N. W., H. Niki, D. Hastie, P. Shepson, P. Roussel, O. Melo, G. Mackay, J. Drummond, H. Schiff, L. Poissant, and W. Moroz, The Southern Ontario oxidant study (SONTOS): Overview and case studies for 1992, *Atmos. Environ.*, *30*, 2125–2132, 1996.

Sceats, M. G., Brownian coagulation in aerosols—The role of long range forces, *J. Colloid Inter. Sci.*, *129*, 105–112, 1989.

Schwartz, S. E., The Whitehouse Effect—shortwave radiative forcing of climate by anthropogenic aerosols: An overview, *J. Aerosol Sci.*, *27*, 359–382, 1996.

Seinfeld, J. S., and S. N. Pandis, *Atmospheric Chemistry and Physics: From Air Pollution to Climate Change*, John Wiley, New York, 1998.

Singh, M. P., R. T. McNider, and J. T. Lin, An analytical study of diurnal wind variations in the boundary layer and the low level nocturnal jet, *Boundary Layer Met.*, *63*, 397–423, 1993.

Stull, R. B., *An Introduction to Boundary Layer Meteorology*, Kluwer, Boston, 1988.

Twomey, S., Aerosols, clouds, and radiation, *Atmos. Environ.*, *25A*, 2435–2442, 1991.

Verheggen, B., and M. Mozurkewich, Observation of a SO_2 induced nucleation event in the atmosphere, *J. Aerosol Sci.*, *29-I*, S609–610, 1998.

Verheggen, B., and M. Mozurkewich, Determination of nucleation and growth rates from measurements of atmospheric aerosol size distributions, *J. Aerosol Sci.*, *31-I*, S446–447, 2000.

Viisanen, Y., M. Kulmala, and A. Laaksonen, Experiments on gas-liquid nucleation of sulfuric acid and water, *J. Chem. Phys.*, *107*, 920–926, 1997.

Weber, R. J., P. H. McMurry, F. L. Eisele, and D. J. Tanner, Measurement of expected nucleation precursor species and 3-500-nm diameter particles at Mauna Loa observatory, Hawaii, *J. Atmos. Sci.*, *58*, 2242–2257, 1995.

Weber, R. J., J. J. Marti, P. H. McMurry, F. L. Eisele, D. J. Tanner, and A. Jefferson, Measurements of new particle formation and ultrafine particle growth rates at a clean continental site, *J. Geophys. Res.*, *102*, 4375–4385, 1997.

Weber, R. J., P. H. McMurry, L. Mauldin, D. J. Tanner, F. L. Eisele, F. J. Brechtel, S. M. Kreidenweis, G. L. Kok, R. D. Schillawski, and D. Baumgardner, A study of new particle formation and growth involving biogenic and trace gas species measured during ACE 1, *J. Geophys. Res.*, *103*, 16,385–16,396, 1998.

Wyslouzil, B. E., J. H. Seinfeld, R. C. Flagan, and K. Okuyama, Binary nucleation in acid-water systems, II, Sulfuric acid-water and a comparison with methanesulfonic acid-water, *J. Chem. Phys.*, *94*, 6842–6850, 1991.

B. Verheggen and M. Mozurkewich, Department of Chemistry and Centre for Atmospheric Chemistry, York University, 4700 Keele Street, Toronto, Ontario M3J 1P3, Canada. (mozurkew@yorku.ca)